Ursolic acid alleviates lipid accumulation by activating the AMPK signaling pathway *in vivo* and *in vitro*

Jing Cheng (iD), Ying Liu, Yaojie Liu, Dong Liu, Yang Liu, Yatu Guo, Zijian Wu, Heyu Li, and Hao Wang

Abstract: The mechanism underlying the effect of ursolic acid (UA) on lipid metabolism remains unclear. This study aimed to explore the mechanisms of UA in reducing lipid accumulation in free fatty acids-cultured HepG2 cells and in high-fat-diet-fed C57BL/6J mice. *In vivo*, UA effectively alleviated liver steatosis and decreased the size of adipocytes in the epididymis. It also significantly decreased the total cholesterol (TC) and triglyceride (TG) contents in the liver and plasma in C57BL/6 mice. *In vitro*, UA (20 μM) significantly reduced lipid accumulation; the intracellular TC contents decreased from 0.078 ± 0.0047 to 0.049 ± 0.0064 μmol/mg protein, and TG contents from 0.133 ± 0.005 to 0.066 ± 0.0047 μmol/mg protein, in HepG2 cells. Furthermore, UA reduced the mRNA expression related to fat synthesis, enhanced the mRNA expression related to adipose decomposition, and dramatically upregulated the protein expression of P-AMPK *in vivo* and *in vitro*. Of note, these protective effects of UA on a high-fat environment were blocked by the AMPK inhibitor (compound C) *in vitro*. In addition, the molecular docking results suggested that UA could be docked to the AMPK protein as an AMPK activator. These results indicated that UA lowered the lipid content probably *via* activating the AMPK signaling pathway, thereby inhibiting lipid synthesis and promoting fat decomposition.

Keywords: adenosine 5'-monophosphate-activated protein kinase, C57BL/6J mice, HepG2 cells, lipid accumulation, ursolic acid

Practical Application: Ursolic acid (UA) widely exists in vegetables and fruits. This study highlighted a lipid-lowing mechanism of UA in HepG2 cells and C57BL/6J mice. The data indicated that UA might be used in lipid-lowering functional foods.

1. INTRODUCTION

Lipid metabolic disorders induce many chronic diseases, including atherosclerosis, cardiovascular, type 2 diabetes, aging, and NAFLD (Radaelli et al., 2018). Some anti-obesity drugs are often used to reduce lipid accumulation, but have many side effects, such as liver dysfunction (Saokaew et al., 2017) or gastrointestinal discomfort (Cavaliere, Floriano, & Medeiros-Neto, 2001). Therefore, natural, safe, and novel small molecules should be explored for reducing liver fat accumulation.

Ursolic acid (UA) (Figure 2a) widely exists in vegetables and fruits, such as *Rosmarinus officinalis* leaves and *Ocimum tenuiflorum* and *Vaccinium vitis-idaea* fruits (Hwang et al., 2013) (the content of UA from different sources is summarized in Table 1) (Bernatoniene et al., 2016; Lopez-Hortas, Perez-Larran, Gonzalez-Munoz, Falque, & Dominguez, 2018), which possess antihyperlipidemic (Li et al., 2014), anti-oxidant (Wang, Gong, et al., 2018), anti-inflammatory (Wang, Li, Deng, Liu, & He, 2018), and hy-

poglycemic properties (Rao et al., 2011). Previous studies found that short-term (8 week) dietary supplementation of UA (50 and 200 mg/kg body weight) could activate peroxisome proliferator-activated receptor alpha (PPARα) to improve lipid and glucose metabolism in mice (Jia et al., 2015). Recent studies also demonstrated the roles of UA in obesity. For example, treating 3T3-L1 adipocytes with UA for 6 weeks could inhibit preadipocyte differentiation by activating the LKB1/AMPK pathway (Liu, Qiao, et al., 2017). Also, Chu et al. (2015) showed that UA could adjust UCP3/AMPK to regulate free fatty acid (FFA) accumulation in skeletal muscle cells. A previous study also showed that supplementing 0.125%, 0.25%, and 0.5% UA (approximately 45, 90, and 180 mg/kg body weight) for 6 weeks alleviated fat accumulation induced by a high-fat diet (HFD) in rats (Li et al., 2014). However, previous studies were mostly based on short-term effects. The mechanism underlying the effect of the long-term supplementation of UA on AMPK signaling pathway in C57BL/6J mice is still unclear.

AMPK, a serine/threonine protein kinase, is a sensor of intracellular energy status. Once activated, AMPK directly phosphorylates multiple downstream genes to control glucose and lipid homeostasis (Alvarez-Suarez et al., 2016). Previous studies showed that AMPK inhibited fatty acid synthesis by preventing fat synthesis-related targets, such as acetyl-CoA carboxylase (ACC), sterol regulatory element-binding protein 1C (SREBP-1C), and fatty acid synthase (FAS), as well as by promoting the fatty acid oxidation-related targets, such as carnitine palmitoyltransferase (CPT-1),
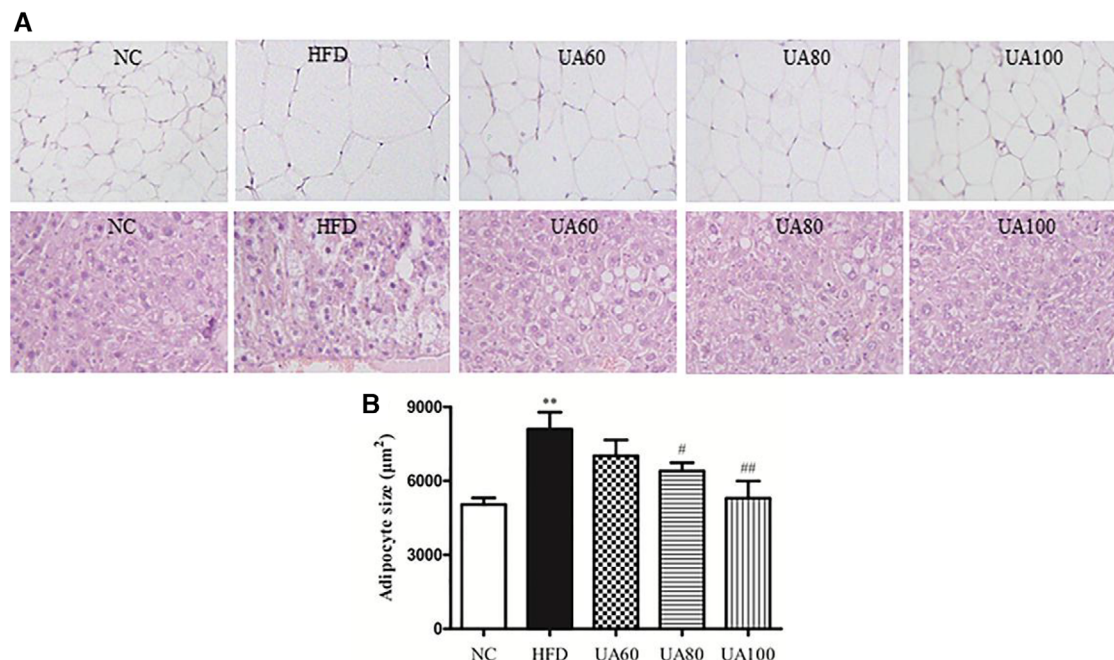
Figure 1–Effect of UA on pathology in EWAT and liver of HFD-administrated mice detected by H&E staining (×200) (a). The adipocyte size of EWAT (b). Data are represented as mean ± SD. **$P < 0.01$ versus control group; #$P < 0.05$ and ##$P < 0.01$ versus FFAs group

Table 1–Content of UA from different sources.

Origin	UA (mg/g)	Origin	UA (mg/g)
Rosmarinus officinalis leaves	15.8 ± 0.2	*Vaccinium vitis-idaea* fruits	7.09
Calendula officinalis flowers	20.53	*Ziziphus jujuba* fruit	0.31 to 0.53
Malus domestica fruit, peel	14.3	*Crataegus pinnatifida* fruits	0.61 to 1.14
Ligustrum lucidum Ait. fruit	5.8 to 9.8	*Satureja montana*	9.4

Note. These data were obtained from previous reports (Bernatoniene et al., 2016; Lopez-Hortas et al., 2018).

acyl-coenzyme A oxidase 1 (ACOX1), and PPARα (Fan et al., 2018).

SREBP-1C can bind to the promoter of downstream genes, such as ACC (Park, Kim, Im, & Lee, 2015) and FAS (Chen et al., 2018). The downregulation of ACC, a rate-limiting enzyme of *de novo* lipogenesis, decreases the synthesis of malonyl-CoA, up-regulates the gene expression of CPT-1, and then promotes fatty acid β-oxidation (Al Zarzour et al., 2017). FAS is another key factor for the synthesis of fatty acids, which catalyzes the conversion of acetyl-CoA and malonyl-CoA into palmitate (Chang et al., 2013). SREBP-2 is relatively specific to cholesterol synthesis; it can adjust the expression of cholesterol synthesis-related genes (e.g., 3-hydroxy-3-methylglutaryl-CoA reductase [HMGCR]) (Yeom et al., 2018). Cluster of differentiation 36 (CD36) is a multifunctional class B scavenger receptor that regulates lipid balance and immune response; it binds to lipids, transports lipids into cells, and then enters the next step of lipid metabolism, such as β-oxidation (Zhao, Varghese, Moorhead, Chen, & Ruan, 2018). PPARα is a nuclear receptor that regulates the expression of genes related to fatty acid oxidation, such as promoting the gene expression of ACOX1 and CPT1. ACOX1 and CPT1 are vital enzymes in peroxisome β oxidation. The deletion of peroxisome β gene leads to the inability of hepatocytes to oxidize long-chain fatty acids and hence lipid accumulation (Zeng et al., 2016).

In this study, HFD-fed C57BL/6J mouse model was used for *in vivo* studies, whereas FFAs-cultured HepG2 cells were used for *in vitro* studies to evaluate the mechanism underlying the lipid-lowing effect of the supplementation of UA on the AMPK pathway, and the protective effect of the long-term supplementation of UA in mice. The purpose of this study was to provide a basis for the development of functional foods containing UA.

2. MATERIALS AND METHODS

2.1 Chemicals

UA (purity ≥90%), compound C, oleate acid (OA), palmitate acid (PA), penicillin, and streptomycin were purchased from Sigma–Aldrich (St Louis, MO, USA). Trypsin, Dulbecco's modified Eagle's medium (DMEM), and fetal bovine serum (FBS) were obtained from Hyclone (Logan, UT, USA). Triglyceride (TG), total cholesterol (TC), and BCA protein assay kits were purchased from Nanjing Jiancheng Bioengineering Institute (Nanjing, China). AMPK, P-AMPK, and β-actin antibody were purchased from Cell Signaling Technology (Danvers, MA, USA). Mineral and vitamin mixes were procured from Harlan Teklad (Madison, WI, USA). Cholesterol was purchased from Solarbio Life Science (Beijing, China), whereas others were obtained from the Tianjin supermarket.
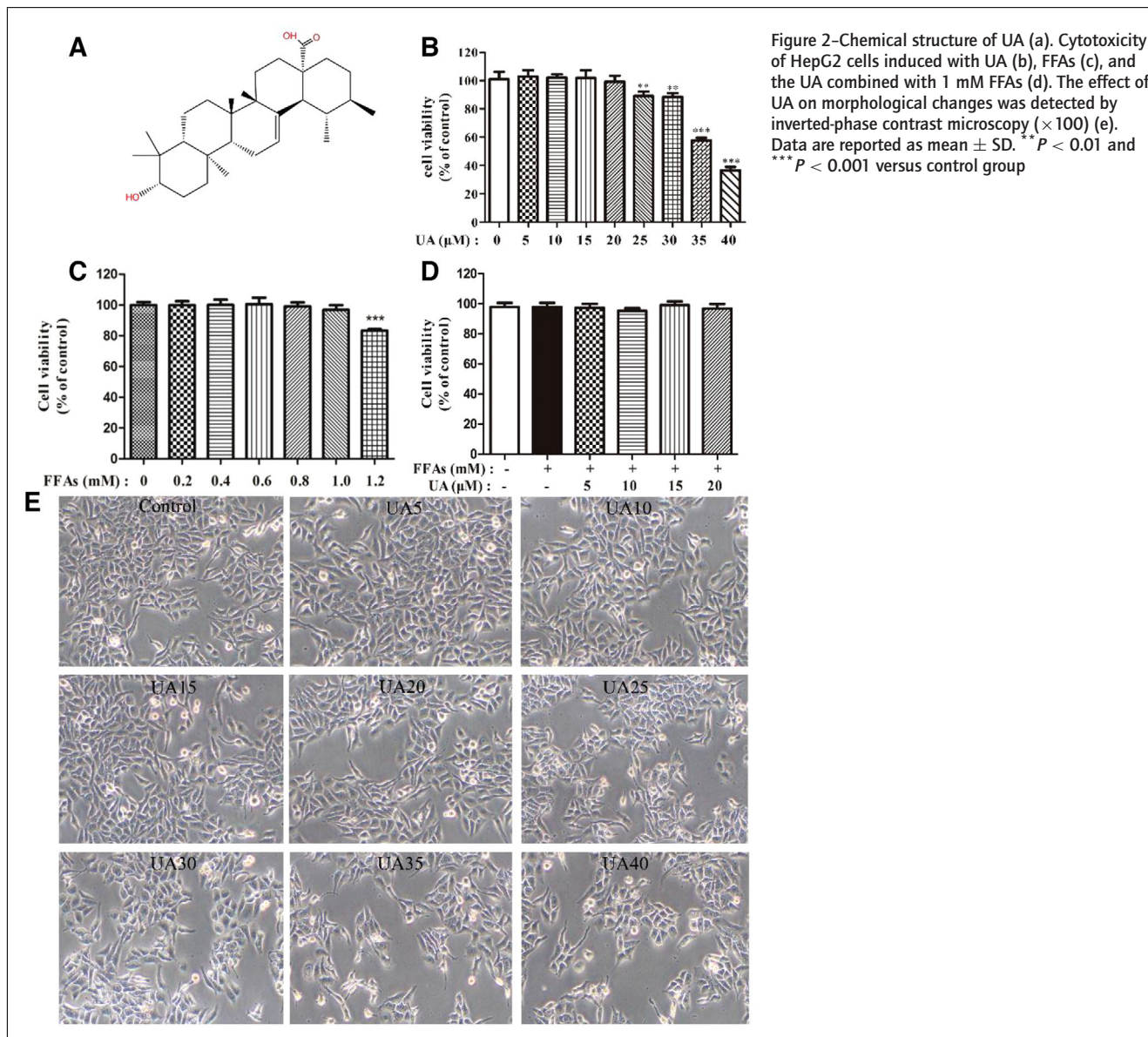
Figure 2–Chemical structure of UA (a). Cytotoxicity of HepG2 cells induced with UA (b), FFAs (c), and the UA combined with 1 mM FFAs (d). The effect of UA on morphological changes was detected by inverted-phase contrast microscopy ($\times$100) (e). Data are reported as mean $\pm$ SD. [**]$P < 0.01$ and [***]$P < 0.001$ versus control group

2.2 | Animal experiment

Male C57BL/6J mice (weighing 19 to 20 g; aged 6 weeks) were obtained from Beijing Vital River Laboratory Animal Technology Co., Ltd. (Beijing, China). A total of 60 mice were housed in normative animal rooms with a specific environment: temperature, 23 ± 2 °C; humidity, $50\% \pm 10\%$; and a 12 hr light/dark cycle. The experiments were performed under the guidelines and approval of the Ethics Committee for the Experimental Use of Animals at the Center for Drug Safety Evaluation of Tianjin University of Science and Technology (Approval No: 20171114C).

The C57BL/6J mice were randomly divided into five groups (12 in each group) for 15 weeks to administer the following diets: normal diet (NC), HFD, and HFD combined with orally administered UA (60, 80, and 100 mg/kg body weight). The dose of UA was according to previous doses (Jia et al., 2015; Zhai et al., 2018). It was equivalent to human doses of 4.86, 6.49, and 8.11 mg/kg body weight per day, as shown in Table 1. This calculation was based on the body surface area, using the following formula: human doses (mg/kg) = mouse dose (mg/kg) $\times$ (3/37), where 3 and

37 mean Km (Km = weight/body surface area) of 0.02 kg mouse and 60 kg human being (Reagan-Shaw, Nihal, & Ahmad, 2008). Humans need the supplementation of 18.45, 24.6, and 30.99 g *Rosmarinus officinalis* leaves or 20.39, 27.23, and 34.03 g *Malus domestica* fruit to reach the doses. The diet was drafted according to the American Institute of Nutrition's 1993 guidelines. The ingredients in the control diet were as follows (g/kg diet): casein, 212; sucrose, 50; vitamin mix, 15; D-L methionine, 1; mineral mix, 35; lard, 50; gelatin, 10; and corn starch, 627. The ingredients in HFD were as follows (g/kg diet): casein, 212; sucrose, 50; vitamin mix, 15; D-L methionine, 1; mineral mix, 35; lard, 200; cholesterol, 1; gelatin, 10; and corn starch, 476.

After a 15-week supplementation, the mice were euthanized humanely, and blood was immediately extracted from the mouse eyeball after withholding food for 12 hr. Blood samples and liver were immediately excised, transferred to liquid nitrogen, and then stored at -80 °C for further analysis. Meanwhile, the tissues were weighed as previously described, frozen in liquid nitrogen, and then stored at -80 °C for further analysis. Moreover, a part of the liver and

Health, Nutrition, & Food

Table 2–Sequence of the primers used in real-time PCR.

Genes		HepG2	Liver
GAPDH	Forward	ATGCTGGTGCCGAGTATGTTGCGAGAAGGTGCGGAGATGATGAC	GCATCTTCTTGTGCAGTGCCTACGGCCAAATCCGTTCACA
	Reverse		
AMPK	Forward	TGAAGCCAGAAACGTGTTGATAATTTGGCGATCCACAGC	GGACTTACTTGTTGGATTTCCGCCTTTGGCAAGATCGATAGTTG
	Reverse		
SREBP-1C	Forward	GTCGTAGATGCGGAGAAGTTGATGGAGGAGCGGGTAG	CTGCTAGCTAGATGACCCTGCTCTGGCTTTGATCCGGAAG
	Reverse		
ACC	Forward	ACTGTGGTGGTTGGTAGAGCGGTTGAAGTCCTTGATGG	GGAGGAGGAGGGGAAAGGGATCTCCCCAAGGAGATACCCCA
	Reverse		
FAS	Forward	GCCGCCATCTACAACATCGTCTTCCACACTATGCTCAG	GTGCTTGCTGGCTCACAGTTAGGTTGGTGTACCCCCATTCA
	Reverse		
SREBP-2	Forward	TCACATTACCTTCCTTCTCCATTACCGTCTGTTGTTG	GTTGACCACGCTGAAGACAGACACCAGGGTTGGCACTTGAA
	Reverse		
HMGCR	Forward	TTCCAGAGCAAGCACATTAGCCCAACTCCAATCACAAGACATTC	GAGCCCATGCATGCTAAGTGCCATGCATCCGGAAAAGTC
	Reverse		
PPARα	Forward	CAGGCTATCATTACGGAGTCCGGTCGCACTTGTCATAC	TGCAGCTCAGCCAAGTTGAATTCCCGAACTTGACCAGCCA
	Reverse		
ACOX1	Forward	CCACTGCCTATGCCTTCCCCATCCGACATGCTTCAATG	TTCGTGCAGCCAGATTGGTAGCGGCTTTGTCTGAATCTTGG
	Reverse		
CPT-1	Forward	TACTTCAAGGTCTGGCTCTACGAGGCTCCGAGGTATTGTC	GCATCTTCTTGTGCAGTGCCTACGGCCAAATCCGTTCACA
	Reverse		
CD36	Forward	GATGAACAGCAGCAACATTCCCACAGCCAGATTGAGAAC	GCCAAGCTATTGCGACATGAATCTCAATGTCCGAGACTTTTCAAC
	Reverse		

epididymal white adipose tissue (EWAT) were fixed in formalin solution for histologic analysis (Cai, Huang, & Wang, 2015; Ye, Wu, Zhang, & Wang, 2019).

2.3 Metabolic parameters analysis

The serum samples were collected and centrifuged at $4,000 \times g$ and 4 °C for 15 min as previously described (Cai et al., 2015). The serum TC, TG, and high-density lipoprotein cholesterol (HDL-C) and the liver TC, TG, and protein levels were measured using enzymatic analysis kits (Nanjing Jiancheng Bioengineering Institute, Nanjing, China) according to the assay protocol and by a previously described method (Chen, Fang, & Wang, 2020). The serum non–HDL-C level was calculated by subtracting the HDL-C level from the TC level.

2.4 Histological analysis

EWAT and liver tissues were embedded in paraffin for hematoxylin and eosin (H&E) straining. The stained images were observed under an inverted microscope (200× magnification). The adipocyte sizes were analyzed using Image J software.

2.5 Cell culture

The human hepatoblastoma cell line (HepG2) was gained from the Cell Resource Center of Shanghai Institute of Life Sciences, Chinese Academy of Sciences. HepG2 cells were grown in DMEM supplemented with 10% FBS, 0.1 U/L penicillin, and 0.1 g/L streptomycin in a humidified incubator at 37 °C with 5% CO_2. When the cells reached 70% confluence, they were induced with UA and FFAs (OA:PA, 2:1, following by the method reported previously [Gomez-Lechon et al., 2007]) or compound C (2 μM, referring to a previous experimental dose [Cheng et al., 2019]) for 24 hr.

2.6 Cytotoxicity assay

The cells (5×10^4/mL) were seeded in 96-well plates, cultivated for 24 hr, and then incubated with FFAs (0.2, 0.4, 0.6, 0.8, 1, and 1.2 mM), UA (5, 10, 15, 20, 25, 30, 35, and 40 μM), or FFAs combined with UA for 24 hr. Thereafter, HepG2 cells were treated with 3-(4,5-dimethylthiazol-2-yl)-2,5-diphenyltetrazolium bromide (MTT) for 4 hr, after which MTT was replaced with 150 μL of Methyl sulfoxide (DMSO). The absorbance was determined with a microplate reader at 570 nm.

2.7 Oil red O staining assay

The oil red O staining assay can reflect intracellular fat content, which can be detected by a previously described method (Cheng et al., 2019). In brief, the cells (5×10^4/mL) were seeded in 96-well plates, cultivated for 24 hr, and then incubated with FFAs and UA for 24 hr. The cells were washed with phosphate buffer saline (PBS) thrice and fixed with paraformaldehyde for 40 min. After 40 min of fixation, the cells were stained with oil red O for 40 min and then observed under an inverted microscope. The cells were washed with 60% isopropanol for 10 s before adding 200 μL isopropanol to dissolve oil red O, so as to determine the content of oil red O. The absorbance was detected with a spectrophotometer at 510 nm.

2.8 Quantification of intracellular TC and TG contents

The TC and TG contents of cells and protein concentrations were measured using commercial kits by the methods described in Section 2.3. Finally, the TG and TC contents were calculated and shown as μmol/mg protein.

Table 3–Body/organ weight of C57BL/6J mice.

Parameters	NC	HFD	UA 60	UA 80	UA 100
Before UA supplement (g)	19.42 ± 0.54	19.39 ± 0.24	19.57 ± 0.38	19.47 ± 0.49	19.32 ± 0.29
After UA supplement (g)	30.12 ± 1.67	38.94 ± 2.84[*]	34.22 ± 1.27[#]	31.35 ± 2.53[#]	30.09 ± 1.82[#]
Food intake (g/day)	3.51 ± 0.67	3.45 ± 0.68	3.52 ± 0.54	3.56 ± 0.71	3.53 ± 0.65
Liver (g)	1.44 ± 0.56	2.82 ± 0.54[*]	2.56 ± 0.76[#]	2.34 ± 0.53[#]	2.03 ± 0.66[#]
Heart (g)	0.18 ± 0.03	0.19 ± 0.02	0.20 ± 0.02	0.19 ± 0.03	0.18 ± 0.02
Kidney (g)	0.41 ± 0.06	0.43 ± 0.07	0.42 ± 0.05	0.45 ± 0.07	0.44 ± 0.06
Perirenal adipose (g)	0.12 ± 0.01	0.48 ± 0.03[*]	0.39 ± 0.02[#]	0.32 ± 0.03[#]	0.23 ± 0.02[#]
Epididymal adipose (g)	2.21 ± 0.25	3.68 ± 0.27[*]	3.51 ± 0.24[#]	3.08 ± 0.32[#]	2.68 ± 0.16[#]

Note. Data are represented as mean ± SD ($n = 12$).
[*]$P < 0.05$ versus control group.
[#]$P < 0.05$ versus FFAs group.

Table 4–Effect of UA on metabolic parameters of C57BL/6J mice.

Parameters	NC	HFD	UA 60	UA 80	UA 100
Serum					
TG (mmol/L)	0.75 ± 0.08	1.32 ± 0.13[**]	1.19 ± 0.09[#]	13 ± 0.06[#]	0.94 ± 0.04[#]
TC (mmol/L)	3.22 ± 0.36	5.75 ± 0.89[**]	5.03 ± 0.76	4.12 ± 0.66[#]	3.72 ± 0.68[#]
HDL-C (mmol/L)	1.71 ± 0.08	1.89 ± 0.13	1.99 ± 0.12	2.22 ± 0.14[#]	2.49 ± 0.18[#]
No-HDL-C (mmol/L)	1.52 ± 0.09	3.85 ± 0.19[**]	3.04 ± 0.13[#]	1.99 ± 0.11[#]	1.23 ± 0.07[##]
Liver					
TG (mmol/g)	1.21 ± 0.07	2.91 ± 0.43[**]	2.15 ± 0.22[#]	1.94 ± 0.12[##]	1.32 ± 0.07[##]
TC (mmol/g)	13 ± 0.09	3.21 ± 0.29[**]	2.75 ± 0.34[#]	2.02 ± 0.18[#]	1.28 ± 0.06[##]

Note. Data are represented as mean ± SD ($n = 12$).
[**]$P < 0.01$ versus control group.
[#]$P < 0.05$.
[##]$P < 0.01$ versus FFAs group.

2.9 Real-time polymerase chain reaction assay

The cells and liver tissue were lysed to obtain total RNA as described previously (Wang et al., 2017; Yang, Cai, Huang, & Wang, 2020). cDNA was synthesized by reverse transcription using a commercial kit (TaKaRa PrimeScript RT Master Mix, Dalian, China) following the manufacturer's protocol. The mRNA expression was detected using UltraSYBR Mixture reagents (CoWin Biosciences, Beijing, China). The related primers are summarized in Table 2. The expression of genes was standardized to the level of glyceraldehyde-3-phosphate dehydrogenase (GAPDH).

2.10 Determination of AMPK activity

AMPK activity was determined in HepG2 cells as described previously to investigate the relationship between AMPK and lipid metabolism (Cheng et al., 2019). An anti-AMPK-panα antibody was purchased from Merck (California, USA.). SAMS peptide (HMRSAMSGLHLVKRR) was obtained from Sigma–Aldrich.

2.11 Western blot analyses

The cells and liver were harvested and lysed using RIPA lysis buffer (containing 1% PMSF [phenylmethanesulfonyl fluoride]). The expression levels of proteins were measured as described previously (Li et al., 2019). The extracted proteins were separated on 10% sodium dodecyl sulfate polyacrylamide gel electrophoresis (SDS-PAGE), and then transferred onto a polyvinylidene difluoride membrane. The membrane was sealed with 3% skimmed milk for 2 hr. For immunoblotting, the blots were hybridized with primary antibodies overnight at 4 °C. Then, the membrane was soaked in the secondary antibody for 1 hr and, the ECL Plus chemiluminescence agent was added. The protein stripes were observed using autoradiography (Kodak, Japan). β-Actin was used as an internal loading control.

2.12 Molecular docking

Molecular docking was conducted using the software of CDOCKER with Discover Studio 3.5 (Accelrys, California, USA), as previously described, to explore the possible interaction mode of UA and AMPK (Cheng et al., 2019). The crystal of AMPK protein (PDB:4CFH) was retrieved from the RCSB Protein Data Bank, and the structure of UA was obtained using the ChemBio3D software.

2.13 Statistical analysis

Data were shown as mean ± standard deviation, and all experiments were repeated at least three times. Significant differences were analyzed by one-way analysis of variance (ANOVA), followed by Duncan's test for *post hoc* analysis. A P-value < 0.05 indicated a statistically significant difference.

3. RESULTS AND DISCUSSION

3.1 UA reduced body and viscera weights and improved profiles of serum and liver

The initial body weights of mice were similar, and the data showed no remarkable differences in the food intake (Table 3). However, the average body weight, liver weight, and epididymal and perirenal adipose contents significantly increased in the HFD group compared with the NC group due to different energy consumption (Table 3) ($P < 0.05$). After administering UA for 15 weeks, the average body weight, liver weight, and epididymal and perirenal adipose contents significantly reduced in the UA (at 100 mg/kg) group by 22.7%, 28%, 27.2%, and 52.1% compared with the HFD group, respectively (all $P < 0.05$). Non-HDL-C is considered to be an important risk factor for predicting obesity-related chronic diseases and is superior to low-density lipoprotein cholesterol in disease assessment (Liu et al., 2018; Ramjee,
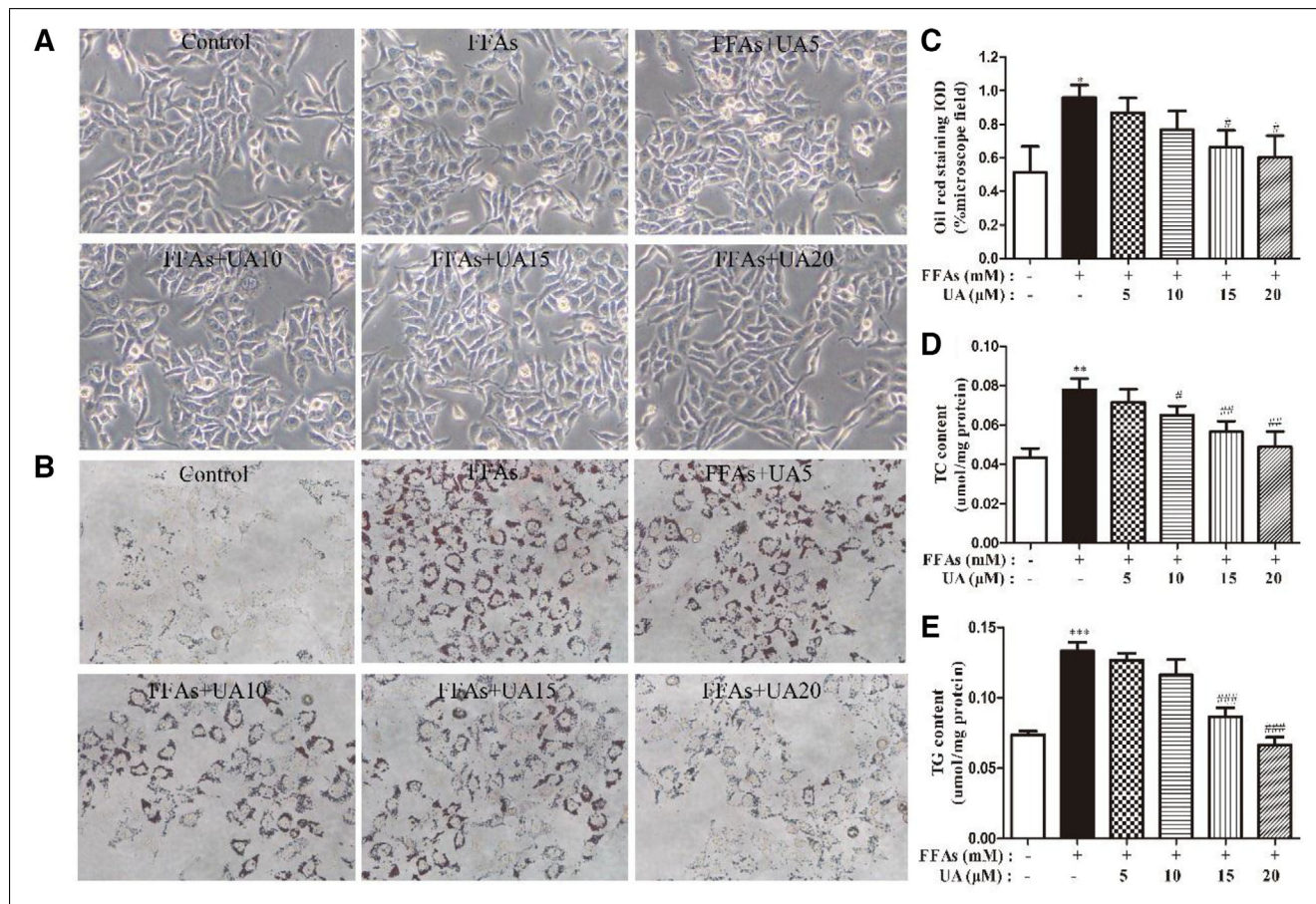
Figure 3–Effect of UA on the lipid content. Morphological changes of HepG2 cells (a) (×100) and oil red O-stained cells (b) (×200) were observed using inverted-phase contrast microscopy. The content of oil red O staining (c) was detected by the colorimetric method. The contents of intracellular TC (d) and TG (e) were measured using commercial kits. The concentration of FFAs was 1 mM. Data are represented as mean ± SD. $^*P < 0.05$, $^{**}P < 0.01$, and $^{***}P < 0.001$ versus control group; $^#P < 0.05$, $^{##}P < 0.01$, and $^{###}P < 0.001$ versus FFAs group

Table 5–Interacting amino acids between macromolecule and ligands.

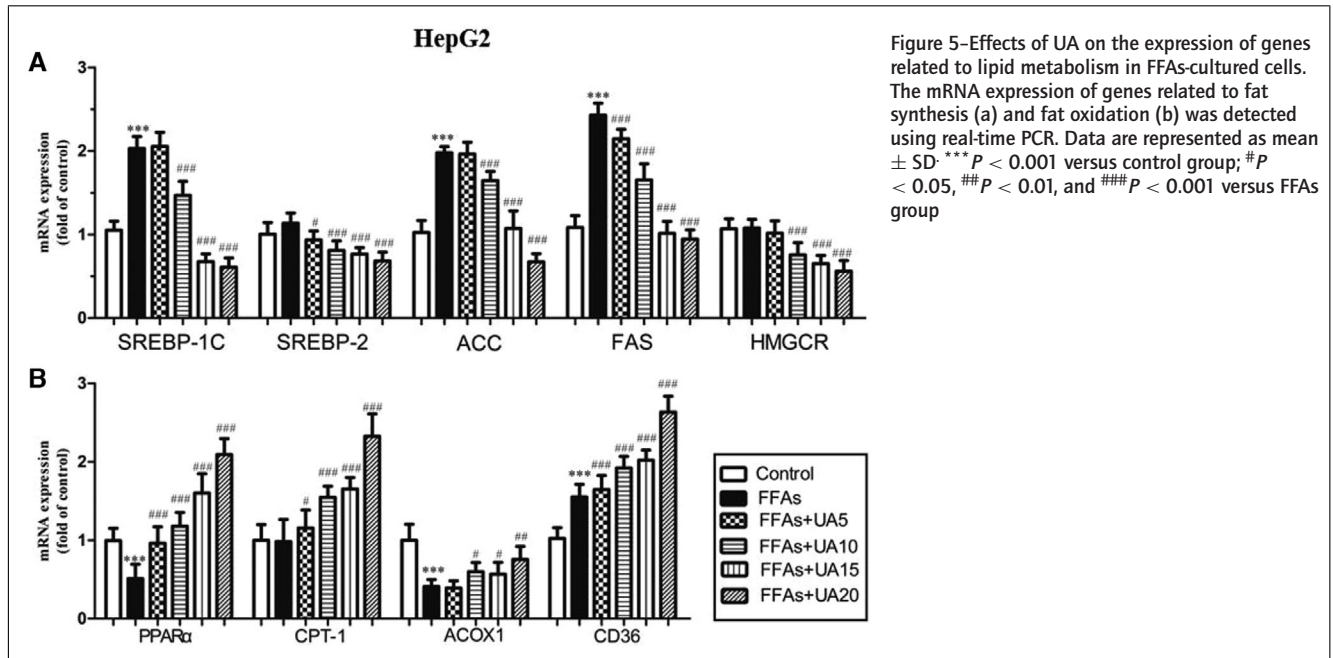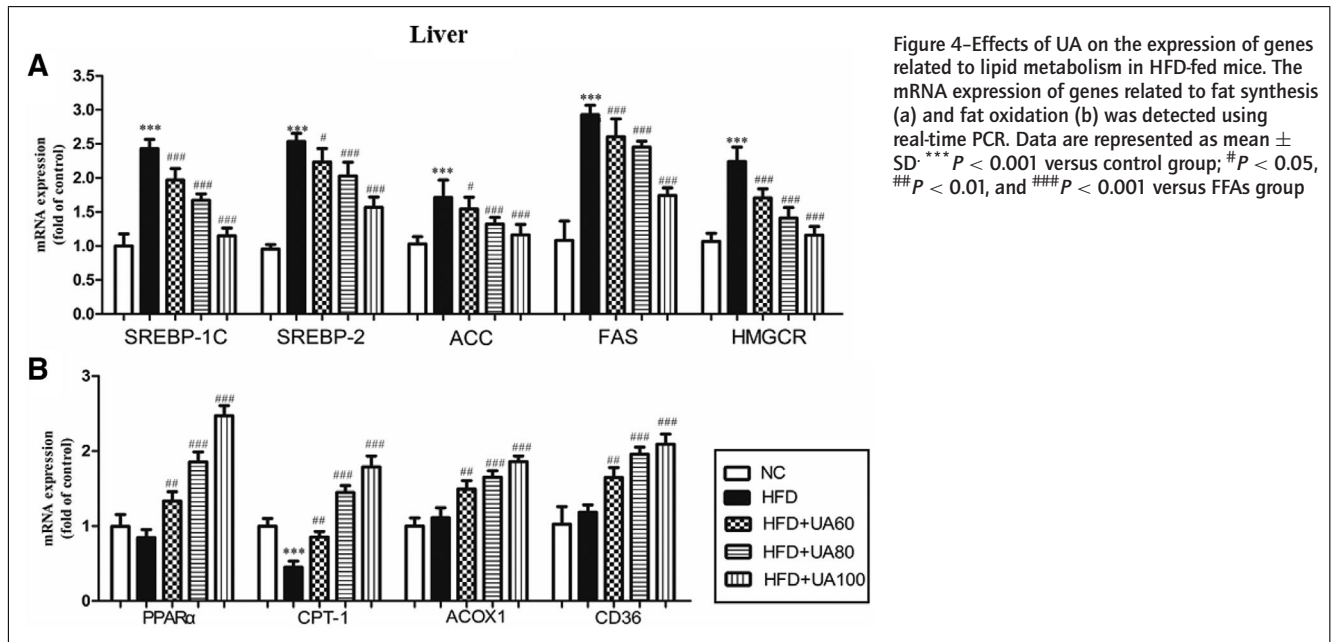| Ligands name	Hydrogen bondsInvolved residues	Binding energy (kcal/mol)	Interactive amino acids
UA	ARG 132ASP 128	−70.02448	MET 334, GLU 232, ARG 331, ASN 335, ASP 128, ARG 132, THR 258, ILE 259, ARG 263, LYS 260, LYS 338, PRO 278, LEU 342, TYR 341, and THR 43
PT1	ARG 263ARG 132	−196.28528	GLU 232, ASN 335, ASP 128, ARG 132, ILE 259, ARG 263, LYS 260, PRO 278, LYS 262, MET 134, HIS 131, and ARG 331

Sperling, & Jacobson, 2011; Verbeek, Hovingh, & Boekholdt, 2015). Therefore, the serum levels of TC, TG, HDL-C, and non-HDL-C and the TC and TG contents in liver tissue were tested to evaluate the lipid-lowering effect of UA (Table 4). The results showed that the serum concentrations of TC, TG, and non-HDL-C, as well as the TC and TG contents in the liver, significantly increased in the HFD group, whereas the serum level of HDL-C was not significantly changed. These data showed that HFD induced lipid accumulation in mice, which was consistent with the findings of Liu, Qiao, et al. (2017). After the supplementation of UA, the liver and serum levels of TC, TG, and non-HDL-C significantly reduced, which was consistent with previous reports showing that the supplementation of UA alleviated the hepatic steatosis by reducing the levels of hepatic TG and TC in HFD-fed mice (Kwon, Shin, & Choi, 2018). Further, the level of serum HDL-C dramatically increased compared with the HFD group. These results showed that UA decreased lipid accumulation in HFD-fed mice.

3.2 Histopathological analysis of mice

In animal experiments, HFD-induced excessive fat accumulation usually leads to marked accumulations of lipids in tissues, such as liver, kidney, and epididymis (Jiao et al., 2019). The morphology of EWAT and liver was analyzed by H&E staining to explore and observe the effects of UA administration on tissue fat accumulation (Figure 1). HFD administration significantly increased the mean size of adipose cells compared with that in the NC group (P < 0.05), whereas the supplementation of UA (at 100 mg/kg) dramatically reduced the mean size of adipose cells compared with that in the HFD group (P < 0.05) (Figure 1). The histopathological analysis of the liver illustrated that HFD treatment exhibited severe liver steatosis and empty lipid vacuoles compared with the

Figure 4–Effects of UA on the expression of genes related to lipid metabolism in HFD-fed mice. The mRNA expression of genes related to fat synthesis (a) and fat oxidation (b) was detected using real-time PCR. Data are represented as mean ± SD. ***$P < 0.001$ versus control group; #$P < 0.05$, ##$P < 0.01$, and ###$P < 0.001$ versus FFAs group

Figure 5–Effects of UA on the expression of genes related to lipid metabolism in FFAs-cultured cells. The mRNA expression of genes related to fat synthesis (a) and fat oxidation (b) was detected using real-time PCR. Data are represented as mean ± SD. ***$P < 0.001$ versus control group; #$P < 0.05$, ##$P < 0.01$, and ###$P < 0.001$ versus FFAs group

NC group, suggesting that HFD treatment induced serious liver fat accumulation *in vivo*. Moreover, the supplementation of UA significantly alleviated liver steatosis and empty lipid vacuoles compared with the HFD group, which was consistent with a previous study showing that carnosic acid alleviated liver steatosis by decreasing lipid accumulation in HFD-fad mice (Song et al., 2018). Taken together, these results suggested that UA alleviated liver lipid accumulation in C57BL/6J mice.

3.3 UA reduced FFAs-induced cytotoxicity in HepG2 cells

The effects of FFAs and UA on cell viability were detected using MTT. As shown in Figure 2b and 2e, the cells treated with the tested doses of UA (5, 10, 15, and 20 μM) had no cytotoxicity, whereas high doses of UA (25, 30, 35, and 40 μM) significantly reduced cell viability ($P < 0.05$). Moreover, the viability of HepG2 cells treated with 1.2 mM FFAs was reduced to approximately 80%, whereas 1 mM FFAs had no cytotoxicity, which was consistent with other studies demonstrating that 1 mM FFAs had no cytotoxicity and could induce lipid accumulation in HepG2 cells (Ai et al., 2015) (Figure 2c). In addition, FFAs (1 mM) combined with UA (5, 10, 15, and 20 μM) did not show any cytotoxic effects (Figure 2d). Based on these results, FFAs (1 mM) and UA (5, 10, 15, and 20 μM) were selected for further experiments.
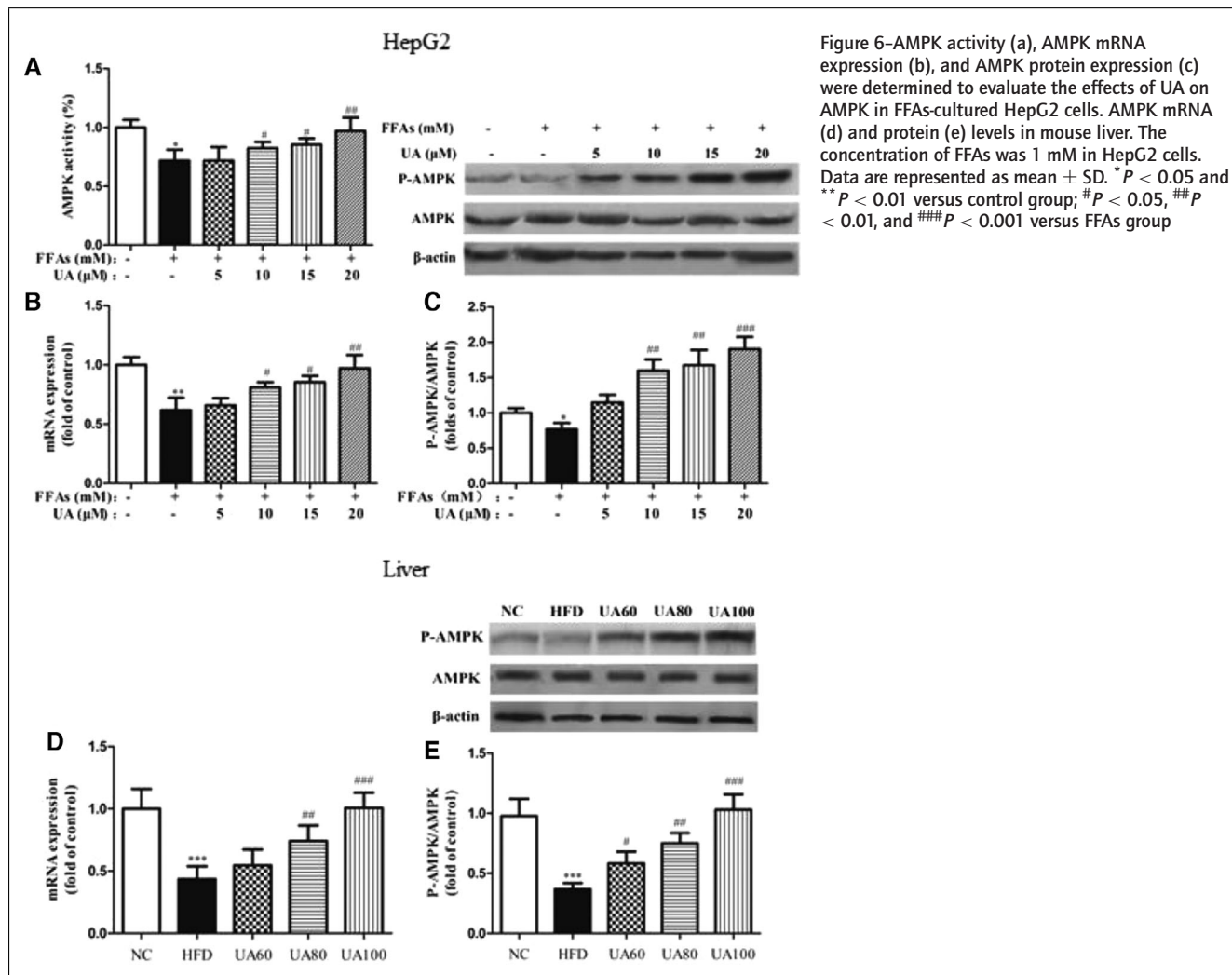
Figure 6–AMPK activity (a), AMPK mRNA expression (b), and AMPK protein expression (c) were determined to evaluate the effects of UA on AMPK in FFAs-cultured HepG2 cells. AMPK mRNA (d) and protein (e) levels in mouse liver. The concentration of FFAs was 1 mM in HepG2 cells. Data are represented as mean ± SD. $^*P < 0.05$ and $^{**}P < 0.01$ versus control group; $^#P < 0.05$, $^{##}P < 0.01$, and $^{###}P < 0.001$ versus FFAs group

3.4 UA suppressed FFAs-induced lipid accumulation in HepG2 cells

FFAs (oleic acid:palmitic acid, 2:1) were added to the medium, and the cells were cultured for 24 hr to significantly induce lipid accumulation. FFAs (1mM) prominently enhanced lipid accumulation (TC and TG contents, $P < 0.05$) compared with the NC group (Figure 2b), which was analyzed by oil red O staining and TC and TG reagent kits ($P < 0.05$) (Figure 3c–e), and was consistent with previous findings (Zhou et al., 2017). However, FFAs had no effect on cell number, yet the cells were round in shape (Figure 3a). UA treatment significantly prevented lipid accumulation ($P < 0.05$) and the increase in intracellular TC and TG contents in FFAs-cultured HepG2 cells (Figure 3). These data demonstrated that UA treatment significantly reversed FFAs-induced lipid accumulation in HepG2 cells. The results of the present study were consistent with other findings indicating a decrease in TC and TG contents, as well as oil red O staining, suggesting that the lipid accumulation decreased in HepG2 cells (Zeng et al., 2016).

3.5 UA prevented lipogenesis and promoted fatty acid oxidation

The present study analyzed the gene expression in the liver of mice (Figure 4). The results showed that HFD significantly enhanced the mRNA expression of ACC, FAS, SREBP-1C, SREBP-2, HMGCR, and CD36 (Figure 4) ($P < 0.05$). Meanwhile, the gene expression of CPT-1 was significantly downregulated ($P < 0.05$). The supplementation of UA dramatically reversed the changes in mRNA expression of genes related to lipogenesis and fatty acid oxidation (all $P < 0.05$).

In vitro, 1 mM FFAs significantly enhanced the expression of ACC, FAS, SREBP-1C, and CD36 (Figure 5) ($P < 0.05$), which was in agreement with a previous study showing that high-fat condition increased the expression of CD36 to promote fatty acid uptake in HepG2 cells (Zang, Fan, Chen, Huang, & Qin, 2018). Meanwhile, the gene expression of ACOX1 and PPARα significantly decreased ($P < 0.05$). Treatment with UA inhibited the mRNA expression of ACC, FAS, SREBP-1C, HMGCR, and SREBP-2 ($P < 0.05$ at 20 μM) (Figure 5a), which was similar to a previous study demonstrating that UA reduced lipid accumulation by suppressing the gene expression of SREBP-1C, FAS, and ACC in T0901317 (LXRα agonist)-induced HepG2 cells (Lin et al., 2018). In addition, UA treatment increased the gene expression of CD36, PPARα, CPT1, and ACOX1 ($P < 0.05$ at 20 μM) (Figure 5b), which was consistent with an earlier study showing that the expressions levels of PPARα and ACOX1 decreased in FFAs–cultured cells to prevent fatty acid β-oxidation (Zang et al., 2018; Zhang et al., 2017). These
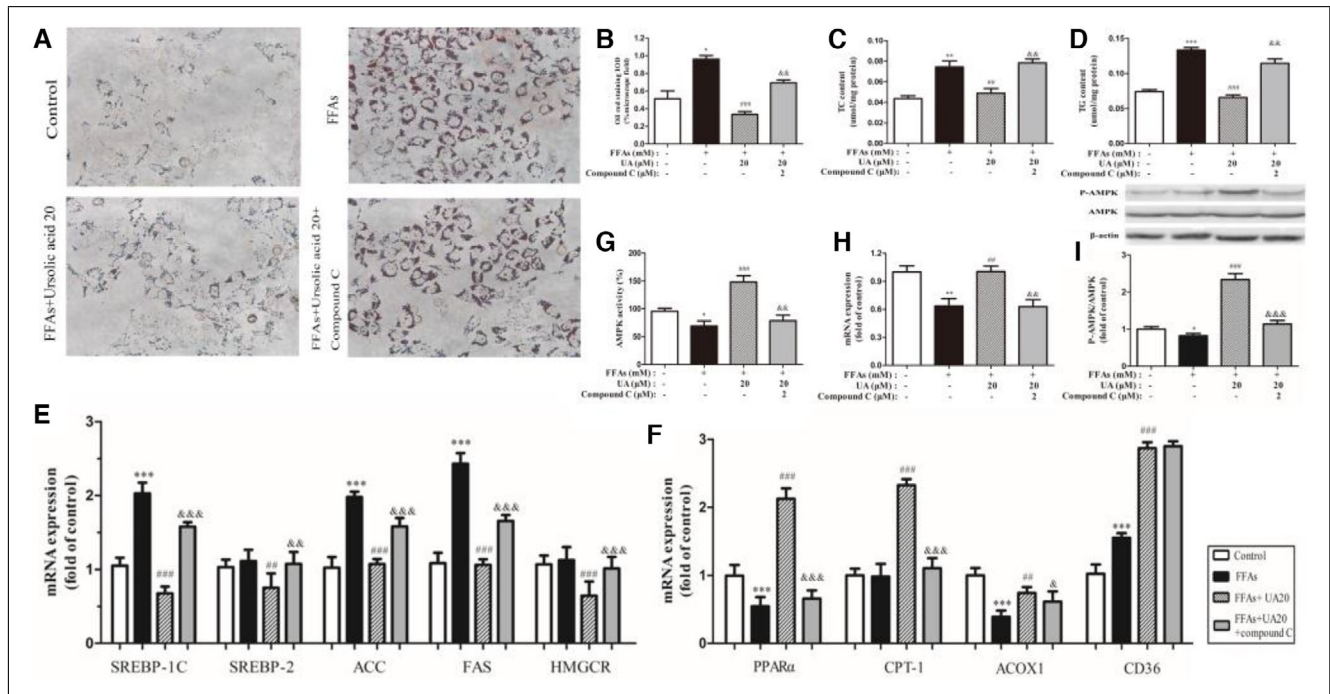
Figure 7–Effects of compound C on UA–FFAs co-cultured HepG2 cells. Oil red O was used to stain fat droplets, and the cells were observed under a microscope (×200) (a). The content of oil red O staining (b), the levels of TG (c) and TC (d), the mRNA expression of genes related to fatty acid synthesis (e) and fatty acid oxidation (f), AMPK activity (g), and AMPK mRNA (h) and protein levels (i) were tested in the presence of compound C. The concentration of FFAs was 1 mM in HepG2 cells. Data are represented as mean ± SD. $^*P < 0.05$, $^{**}P < 0.01$, and $^{***}P < 0.001$ versus control group; $^{##}P < 0.01$ and $^{###}P < 0.001$ versus FFAs group; $^{\&}P < 0.05$, $^{\&\&}P < 0.01$, and $^{\&\&\&}P < 0.001$ versus UA + FFAs group

results showed that UA decreased lipid accumulation by decreasing lipogenesis and increasing lipolysis *in vivo* and *in vitro*.

3.6 UA upregulated the activity and gene and protein expression of AMPK

AMPK can be characterized as a regulator of energy metabolism that can control glucose and lipid homeostasis (Liu, Xu, et al., 2017). *In vitro*, FFAs significantly reduced AMPK activity ($P < 0.05$) and mRNA expression (Figure 6a and 6b) ($P < 0.05$). However, the supplementation of UA reversed the decreased AMPK activity and mRNA expression ($P < 0.05$ at 20 µM). Consistently, the expression levels of P-AMPK protein were observably enhanced (Figure 6c) ($P < 0.05$ at 20 µM) in FFAs-cultured HepG2 cells. These results were in agreement with previous finding that theaflavins enhanced the gene and protein expression of AMPK to reduce hepatic lipid accumulation (Lin, Huang, & Lin, 2007).

Meanwhile, the effects of UA on AMPK gene and protein expression were determined *in vivo* (Figure 6d and 6e). After 15 weeks of UA administration, the gene expression of AMPK in the liver (Figure 6d) and the protein expression of P-AMPK significantly increased ($P < 0.05$ at 80 and 100 mg/kg). These data indicated that UA reduced fatty deposits *via* activating AMPK expression in FFAs-cultured HepG2 cells and HFD-fed C57BL/6J mice. This study was novel in exploring the lipid-lowing property of UA in FFAs-cultured HepG2 cells and HFD-fed C57BL/6J mice based on the AMPK pathway.
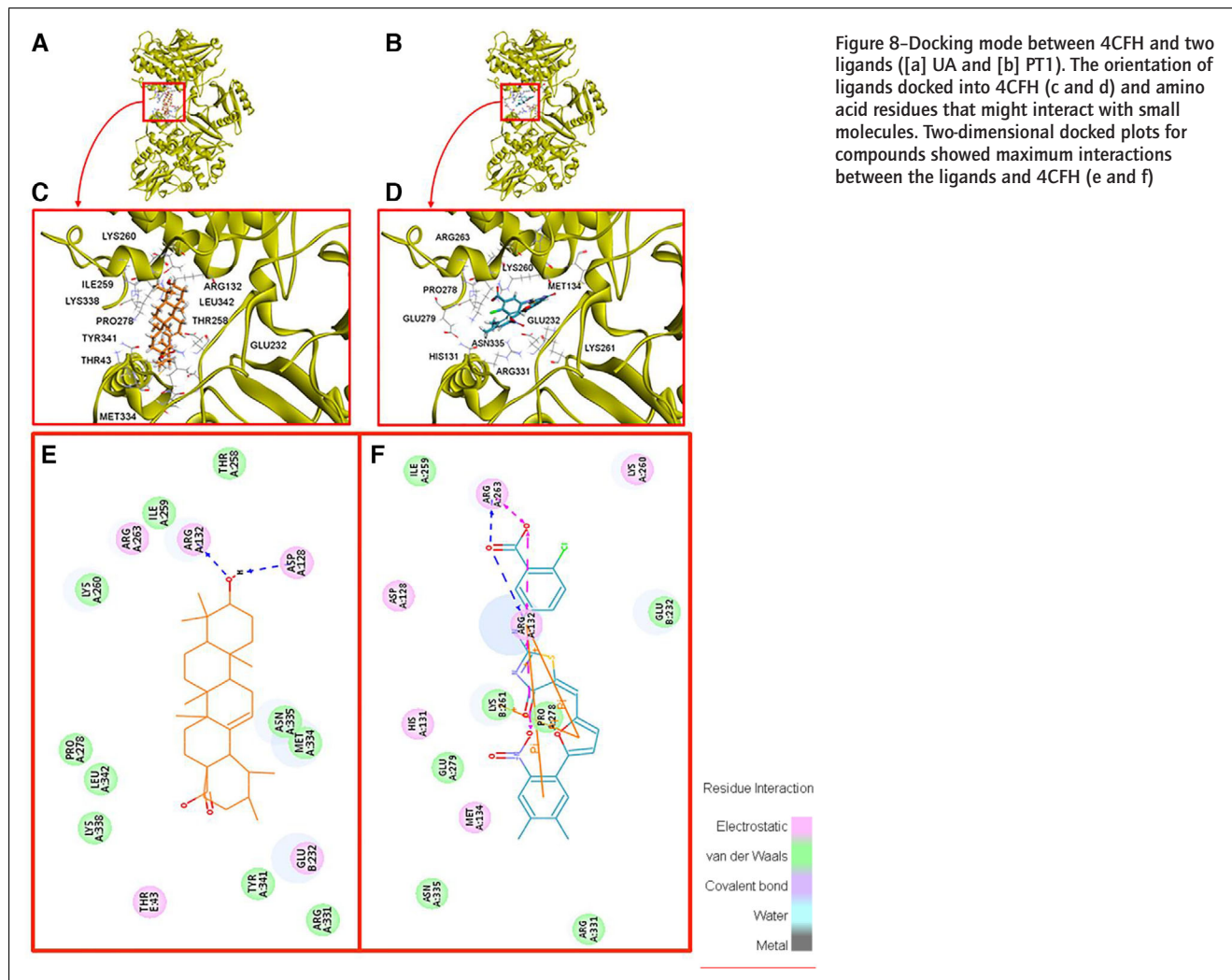
3.7 Compound C reversed the protective effects of UA

Compound C is a potent ATP-competitive inhibitor of AMPK. Therefore, compound C can influence AMPK expression by affecting the AMP/ATP ratio. A previous study indicated that the

increased ratio of AMP/ATP activated AMPK protein (Vila et al., 2011). Also, compound C inhibited the expression of AMPK gene and phosphorylated protein (Lew et al., 2018; Liu, Wang, Hou, Xiong, & Zhao, 2017). The decrease in the number of lipid droplets (Figure 7a and 7b) and TC (Figure 7c) and TG (Figure 7d) contents was abolished by co-treatment with compound C (2 µM) for 24 hr compared with the UA treatment group (all $P < 0.05$). In addition, the decreased gene expression of SREBP-2, FAS, SREBP-1C, ACC, and HMGCR was enhanced (all $P < 0.05$). Meanwhile, the increased mRNA expression of PPARα, CPT-1, and ACOX1 was alleviated (all $P < 0.05$) (Figure 7e and 7f). Astragaloside IV attenuated lipid accumulation by stimulating AMPK and reducing the expression levels of ACC, SREBP-1C, and FAS, and these effects could be reversed by compound C (Zhou et al., 2017). However, treatment with compound C had no effect on the gene expression of CD36 compared with UA-treated cells. Furthermore, the increased AMPK activity (Figure 7g), AMPK gene expression level (Figure 7h), and P-AMPK protein expression level (Figure 7i) were decreased by compound C. These results showed that UA regulated lipid metabolism in FFAs-cultured HepG2 cells partly by activating AMPK.

3.8 Molecular docking

A previous study showed that UA entered the plasma within about 0.5 hr after oral administration of UA (10 mg/kg) in rats; was then transported to organs, such as lung, spleen, and liver; and might bind to some target proteins in organs (Chen, Luo, Zhang, & Chen, 2011). Therefore, molecular docking was used to explore the binding modes of ligands (UA) to responsive sites (AMPK) (Figure 8). UA and PT1 (an activator of AMPK) (Huang et al., 2015; Pang et al., 2008) were docked into 4CFH (Figure 8a and 8b). UA showed good binding energy docked into 4CFH in the

Figure 8–Docking mode between 4CFH and two ligands ([a] UA and [b] PT1). The orientation of ligands docked into 4CFH (c and d) and amino acid residues that might interact with small molecules. Two-dimensional docked plots for compounds showed maximum interactions between the ligands and 4CFH (e and f)

binding pocket, which was comparable to that of PT1. The binding energy was −70.024 kcal/mol (UA) and −196.285 kcal/mol (PT1). In molecular docking, the amino acids that interacted with UA were MET 334, GLU 232, ARG 331, ASN 335, ASP 128, ARG 132, THR 258, ILE 259, ARG 263, LYS 260, LYS 338, PRO 278, LEU 342, TYR 341, and THR 43, and the amino acids that interacted with PT1 were GLU 232, ASN 335, ASP 128, ARG 132, ILE 259, ARG 263, LYS 260, PRO 278, LYS 262, MET 134, HIS 131, and ARG 331. The results showed that UA and PT1 interacted with the AMPK protein *via* nine common amino acids, including GLU 232, ARG 331, ASN 335, ASP 128, ARG 132, ILE 259, ARG 263, LYS 260, and PRO 278. The result revealed that UA could form hydrogen bonds with ARG132 and ASP128 at distance of 8.340 and 2.843 Å, respectively. Meanwhile, PT1 interacted with the ARG263 and ARG132 to form hydrogen bonds (Figure 8 and Table 5). In this situation, the oxygen atom on hydroxyl groups of UA formed multiple hydrogen bonds with some amino acids. Taken together, these results showed that UA and PT 1 bound to the AMPK protein in the same manner, thereby activating AMPK activity. The binding energy, interactive amino acids, and hydrogen bonds involving residues are displayed in Table 5. The results indicated that the binding sites of UA and PT1 were in similar pockets of 4CFH, thus leading to AMPK activation.

4. CONCLUSIONS

This study demonstrated a protective effect of UA against lipid accumulation in FFAs-cultured HepG2 cells and HFD-fed C57BL/6J mice. Furthermore, it indicated that UA regulated lipid metabolism, and this beneficial effect was associated with reduced lipogenesis and increased lipolysis *via* activating the AMPK signaling pathway. These findings indicated that the supplementation with UA might be an advisable strategy for lipid-lowering functional foods to relieve HFD-induced liver injury.

AUTHOR CONTRIBUTIONS

Hao Wang, Zijian Wu, Heyu Li, Yatu Guo, Yang Liu, and Jing Cheng designed this study and interpreted the results. Jing Cheng, Ying Liu, Yaojie Liu, and Dong Liu executed this study and drafted the manuscript.

CONFLICTS OF INTEREST

The authors declare no conflicts of interest.

REFERENCES

Ai, L., Xu, Q., Wu, C., Wang, X., Chen, Z., Su, D., … Fan, Z. (2015). A20 Attenuates FFAs-induced lipid accumulation in nonalcoholic steatohepatitis. *International Journal of Biological Sciences*, 11(12), 1436–1446. https://doi.org/10.7150/ijbs.13371

Al Zarzour, H., R., Ahmad, M., Asmawi, M. Z., Kaur, G., Saeed, M. A. A., … Yam, M. (2017). *Phyllanthus niruri* standardized extract alleviates the progression of non-alcoholic fatty liver disease and decreases atherosclerotic risk in Sprague-Dawley rats. *Nutrients*, 9(7), 766. https://doi.org/10.3390/nu9070766

Alvarez-Suarez, J. M., Giampieri, F., Cordero, M., Gasparrini, M., Forbes-Hernández, T. Y., Mazzoni, L., … Battino, M. (2016). Activation of AMPK/Nrf2 signalling by Manuka honey protects human dermal fibroblasts against oxidative damage by improving antioxidant response and mitochondrial function promoting wound healing. *Journal of Functional Foods*, 25, 38–49. https://doi.org/10.1016/j.jff.2016.05.008

Bernatoniene, J., Cizauskaite, U., Ivanauskas, L., Jakstas, V., Kalveniene, Z., & Kopustinskiene, D. M. (2016). Novel approaches to optimize extraction processes of ursolic, oleanolic and rosmarinic acids from Rosmarinus officinalis leaves. *Industrial Crops and Products*, 84, 72–79. https://doi.org/10.1016/j.indcrop.2016.01.031

Cai, X., Huang, Q., & Wang, S. (2015). Isolation of a novel lutein-protein complex from *Chlorella vulgaris* and its functional properties. *Food & Function*, 6(6), 1893–1899. https://doi.org/10.1039/c4fo01096e

Cavaliere, H., Floriano, I., & Medeiros-Neto, G. (2001). Gastrointestinal side effects of orlistat may be prevented by concomitant prescription of natural fibers (psyllium mucilloid). *International Journal of Obesity*, 25(7), 1095–1099. https://doi.org/10.1038/sj.ijo.0801645

Chang, J. J., Hsu, M. J., Huang, H. P., Chung, D. J., Chang, Y. C., & Wang, C. J. (2013). Mulberry anthocyanins inhibit oleic acid induced lipid accumulation by reduction of lipogenesis and promotion of hepatic lipid clearance. *Journal of Agricultural and Food Chemistry*, 61(25), 6069–6076. https://doi.org/10.1021/jf401171k

Chen, A., Chen, X., Cheng, S., Shu, L., Yan, M., Yao, L., … Liu, G. (2018). FTO promotes SREBP1c maturation and enhances CIDEC transcription during lipid accumulation in HepG2 cells. *Biochimica et Biophysica Acta (BBA) - Molecular and Cell Biology of Lipids*, 1863(5), 538–548. https://doi.org/10.1016/j.bbalip.2018.02.003

Chen, Q., Luo, S., Zhang, Y., & Chen, Z. (2011). Development of a liquid chromatography-mass spectrometry method for the determination of ursolic acid in rat plasma and tissue: Application to the pharmacokinetic and tissue distribution study. *Analytical and Bioanalytical Chemistry*, 399(8), 2877–2884. https://doi.org/10.1007/s00216-011-4651-x

Chen, X., Fang, F., & Wang, S. (2020). Physicochemical properties and hepatoprotective effects of glycated Snapper fish scale peptides conjugated with xylose via Maillard reaction. *Food and Chemical Toxicology*, 137, 111115. https://doi.org/10.1016/j.fct.2020.111115

Cheng, J., Liu, D., Zhao, J., Li, X., Yan, Y., Wu, Z., … Wang, C. (2019). Lutein attenuates oxidative stress and inhibits lipid accumulation in free fatty acids-induced HepG2 cells by activating the AMPK pathway. *Journal of Functional Foods*, 60, 103445. https://doi.org/10.1016/j.jff.2019.103445

Chu, X., He, X., Shi, Z., Li, C., Guo, F., Li, S., … Sun, C. (2015). Ursolic acid increases energy expenditure through enhancing free fatty acid uptake and beta-oxidation via an UCP3/AMPK-dependent pathway in skeletal muscle. *Molecular Nutrition & Food Research*, 59(8), 1491–1503. https://doi.org/10.1002/mnfr.201400670

Fan, X. X., Leung, E. L., Xie, Y., Liu, Z. Q., Zheng, Y. F., Yao, X. J., … Liu, L. (2018). Suppression of lipogenesis via reactive oxygen species–AMPK signaling for treating malignant and proliferative diseases. *Antioxidants & Redox Signaling*, 28(5), 339–357. https://doi.org/10.1089/ars.2017.7090

Gomez-Lechon, M. J., Donato, M. T., Martinez-Romero, A., Jimenez, N., Castell, J. V., & O'Connor, J. E. (2007). A human hepatocellular in vitro model to investigate steatosis. *Chemico-Biological Interactions*, 165(2), 106–116. https://doi.org/10.1016/j.cbi.2006.11.004

Huang, L., Dai, K., Chen, M., Zhou, W., Wang, X., Chen, J., & Zhou, W. (2015). The AMPK agonist PT1 and mTOR inhibitor 3HOI-BA-01 protect cardiomyocytes after ischemia through induction of autophagy. *Journal of Cardiovascular Pharmacology & Therapeutics*, 21(1), 71–84. https://doi.org/10.1177/1074248415581177

Hwang, Y. P., Kim, H. G., Choi, J. H., Do, M. T., Chung, Y. C., Jeong, T. C., & Jeong, H. G. (2013). S-allyl cysteine attenuates free fatty acid-induced lipogenesis in human HepG2 cells through activation of the AMP-activated protein kinase-dependent pathway. *The Journal of Nutritional Biochemistry*, 24(8), 1469–1478. https://doi.org/10.1016/j.jnutbio.2012.12.006

Jia, Y., Kim, S., Kim, J., Kim, B., Wu, C., Lee, J. H., … Lee, S. J. (2015). Ursolic acid improves lipid and glucose metabolism in high-fat-fed C57BL/6J mice by activating peroxisome proliferator-activated receptor alpha and hepatic autophagy. *Molecular Nutrition & Food Research*, 59(2), 344–354. https://doi.org/10.1002/mnfr.201400399

Jiao, X., Wang, Y., Lin, Y., Lang, Y., Li, E., Zhang, X., … Li, B. (2019). Blueberry polyphenols extract as a potential prebiotic with anti-obesity effects on C57BL/6 J mice by modulating the gut microbiota. *The Journal of Nutritional Biochemistry*, 64, 88–100. https://doi.org/10.1016/j.jnutbio.2018.07.008

Kwon, E. Y., Shin, S. K., & Choi, M. S. (2018). Ursolic acid attenuates hepatic steatosis, fibrosis, and insulin resistance by modulating the circadian rhythm pathway in diet-induced obese mice. *Nutrients*, 10(11), 1719. https://doi.org/10.3390/nu10111719

Lew, L. C., Choi, S. B., Khoo, B. Y., Sreenivasan, S., Ong, K. L., & Liong, M. T. (2018). *Lactobacillus plantarum* DR7 reduces cholesterol via phosphorylation of AMPK that down-regulated the mRNA expression of HMG-CoA reductase. *Korean Journal for Food Science of Animal Resources*, 38(2), 350–361. https://doi.org/10.5851/kosfa.2018.38.2.350

Li, S., Liao, X., Meng, F., Wang, Y., Sun, Z., Guo, F., … Sun, C. (2014). Therapeutic role of ursolic acid on ameliorating hepatic steatosis and improving metabolic disorders in high-fat diet-induced non-alcoholic fatty liver disease rats. *PLoS One*, 9(1), e86724. https://doi.org/10.1371/journal.pone.0086724

Li, X., Wang, H., Wang, T., Zheng, F., Wang, H., & Wang, C. (2019). Dietary wood pulp-derived sterols modulation of cholesterol metabolism and gut microbiota in high-fat-diet-fed hamsters. *Food & Function*, 10(2), 775–785. https://doi.org/10.1039/c8fo02271b

Lin, C. L., Huang, H. C., & Lin, J. K. (2007). Theaflavins attenuate hepatic lipid accumulation through activating AMPK in human HepG2 cells. *Journal of Lipid Research*, 48(11), 2334–2343. https://doi.org/10.1194/jlr.M700128-JLR200

Lin, Y. N., Wang, C. C. N., Chang, H. Y., Chu, F. Y., Hsu, Y. A., Cheng, W. K., … Lim, Y. P. (2018). Ursolic acid, a novel liver X receptor α (LXRα) antagonist inhibiting ligand-induced nonalcoholic fatty liver and drug-induced lipogenesis. *Journal of Agricultural and Food Chemistry*, 66(44), 11647–11662. https://doi.org/10.1021/acs.jafc.8b04116

Liu, H. X., Xu, M. Q., Li, S. P., Tian, S., Guo, M. X., Qi, J. Y., … Zhao, X. S. (2017). Jujube leaf green tea extracts inhibits hepatocellular carcinoma cells by activating AMPK. *Oncotarget*, 8(66), 110566–110575. https://doi.org/10.18632/oncotarget.22821

Liu, L., Li, Q., Yuan, Z., Zhao, M., Zhang, X., Zhang, H., … The Reaction Study Group.(2018). Non-high-density lipoprotein cholesterol is more informative than traditional cholesterol indices in predicting diabetes risk for women with normal glucose tolerance. *Journal of Diabetes Investigation*, 9(6), 1304–1311. https://doi.org/10.1111/jdi.12837

Liu, X., Wang, Y., Hou, L., Xiong, Y., & Zhao, S. (2017). Fibroblast growth factor 21 (FGF21) promotes formation of aerobic myofibers via the FGF21-SIRT1-AMPK-PGC1alpha pathway. *Journal of Cellular Physiology*, 232(7), 1893–1906. https://doi.org/10.1002/jcp.25735

Liu, Z., Qiao, Q., Sun, Y., Chen, Y., Ren, B., & Liu, X. (2017). Sesamol ameliorates diet-induced obesity in C57BL/6J mice and suppresses adipogenesis in 3T3-L1 cells via regulating mitochondria-lipid metabolism. *Molecular Nutrition & Food Research*, 61(8), 1600717. https://doi.org/10.1002/mnfr.201600717

Lopez-Hortas, L., Perez-Larran, P., Gonzalez-Munoz, M. J., Falque, E., & Dominguez, H. (2018). Recent developments on the extraction and application of ursolic acid. A review. *Food Research International*, 103, 130–149. https://doi.org/10.1016/j.foodres.2017.10.028

Pang, T., Zhang, Z. S., Gu, M., Qiu, B. Y., Yu, L. F., Cao, P. R., … Li, J. (2008). Small molecule antagonizes autoinhibition and activates AMP-activated protein kinase in cells. *Journal of Biological Chemistry*, 283(23), 16051–16060. https://doi.org/10.1074/jbc.M710114200

Park, J. Y., Kim, Y., Im, J. A., & Lee, H. (2015). Oligonol suppresses lipid accumulation and improves insulin resistance in a palmitate-induced in HepG2 hepatocytes as a cellular steatosis model. *BMC Complementary and Alternative Medicine*, 15, 185. https://doi.org/10.1186/s12906-015-0709-1

Radaelli, M. G., Martucci, F., Perra, S., Accornero, S., Castoldi, G., Lattuada, G., … Perseghin, G. (2018). NAFLD/NASH in patients with type 2 diabetes and related treatment options. *Journal of Endocrinological Investigation*, 41(5), 509–521. https://doi.org/10.1007/s40618-017-0799-3

Ramjee, V., Sperling, L. S., & Jacobson, T. A. (2011). Non-high-density lipoprotein cholesterol versus apolipoprotein B in cardiovascular risk stratification: Do the math. *Journal of the American College of Cardiology*, 58(5), 457–463. https://doi.org/10.1016/j.jacc.2011.05.009

Rao, V. S., de Melo, C. L., Queiroz, M. G., Lemos, T. L., Menezes, D. B., Melo, T. S., & Santos, F. A. (2011). Ursolic acid, a pentacyclic triterpene from *Sambucus australis*, prevents abdominal adiposity in mice fed a high-fat diet. *Journal of Medicinal Food*, 14(11), 1375–1382. https://doi.org/10.1089/jmf.2010.0267

Reagan-Shaw, S., Nihal, M., & Ahmad, N. (2008). Dose translation from animal to human studies revisited. *The FASEB Journal*, 22(3), 659–661. https://doi.org/10.1096/fj.07-9574LSF

Saokaew, S., Kanchanasuwan, S., Apisarnthanarak, P., Charoenson, A., Charatcharoenwitthaya, P., Phisalprapa, P., & Chaiyakunapruk, N. (2017). Clinical risk scoring for predicting non-alcoholic fatty liver disease in metabolic syndrome patients (NAFLD-MS score). *Liver International*, 37(10), 1535–1543. https://doi.org/10.1111/liv.13413

Song, H. M., Li, X., Liu, Y. Y., Lu, W. P., Cui, Z. H., Zhou, L., … Zhang, H. M. (2018). Carnosic acid protects mice from high-fat diet-induced NAFLD by regulating MARCKS. *International Journal of Molecular Medicine*, 42(1), 193–207. https://doi.org/10.3892/ijmm.2018.3593

Verbeek, R., Hovingh, G. K., & Boekholdt, S. M. (2015). Non-high-density lipoprotein cholesterol: Current status as cardiovascular marker. *Current Opinion in Lipidology*, 26(6), 502–510. https://doi.org/10.1097/MOL.0000000000000237

Vila, L., Roglans, N., Perna, V., Sanchez, R. M., Vazquez-Carrera, M., Alegret, M., & Laguna, J. C. (2011). Liver AMP/ATP ratio and fructokinase expression are related to gender differences in AMPK activity and glucose intolerance in rats ingesting liquid fructose. *The Journal of Nutritional Biochemistry*, 22(8), 741–751. https://doi.org/10.1016/j.jnutbio.2010.06.005

Wang, H. L., Sun, Z. O., Rehman, R. U., Wang, H., Wang, Y. F., & Wang, H. (2017). Rosemary extract-mediated lifespan extension and attenuated oxidative damage in drosophila melanogaster fed on high-fat diet. *Journal of Food Science*, 82(4), 1006–1011. https://doi.org/10.1111/1750-3841.13656

Wang, X. T., Gong, Y., Zhou, B., Yang, J. J., Cheng, Y., Zhao, J. G., & Qi, M. Y. (2018). Ursolic acid ameliorates oxidative stress, inflammation and fibrosis in diabetic cardiomyopathy rats. *Biomedicine & Pharmacotherapy*, 97, 1461–1467. https://doi.org/10.1016/j.biopha.2017.11.032

Wang, Y., Li, L., Deng, S., Liu, F., & He, Z. (2018). Ursolic acid ameliorates inflammation in cerebral ischemia and reperfusion injury possibly via high mobility group box 1/toll-like receptor 4/NFκB pathway. *Frontiers in Neurology*, 9, 253. https://doi.org/10.3389/fneur.2018.00253

Yang, Q., Cai, X., Huang, M., & Wang, S. (2020). A specific peptide with immunomodulatory activity from *Pseudostellaria heterophylla* and the action mechanism. *Journal of Functional Foods*, 68, 103887. https://doi.org/10.1016/j.jff.2020.103887

Ye, Q., Wu, X., Zhang, X., & Wang, S. (2019). Organic selenium derived from chelation of soybean peptide-selenium and its functional properties in vitro and in vivo. *Food & Function*, 10(8), 4761–4770. https://doi.org/10.1039/c9fo00729f

Yeom, M., Park, J., Lee, B., Lee, H. S., Park, H. J., Won, R., … Hahm, D. H. (2018). Electroacupuncture ameliorates poloxamer 407-induced hyperlipidemia through suppressing hepatic SREBP-2 expression in rats. *Life Sciences*, 203, 20–26. https://doi.org/10.1016/j.lfs.2018.04.016

Zang, Y., Fan, L., Chen, J., Huang, R., & Qin, H. (2018). Improvement of lipid and glucose metabolism by capsiate in palmitic acid-treated HepG2 Cells via Activation of the AMPK/SIRT1 signaling pathway. *Journal of Agricultural and Food Chemistry*, 66(26), 6772–6781. https://doi.org/10.1021/acs.jafc.8b01831

Zeng, L., Tang, W., Yin, J., Feng, L., Li, Y., Yao, X., & Zhou, B. (2016). Alisol A 24-acetate prevents hepatic steatosis and metabolic disorders in HepG2 cells. *Cellular Physiology and Biochemistry*, 40(3-4), 453–464. https://doi.org/10.1159/000452560

Zhai, M., Guo, J., Ma, H., Shi, W., Jou, D., Yan, D., … Lin, L. (2018). Ursolic acid prevents angiotensin II-induced abdominal aortic aneurysm in apolipoprotein E-knockout mice. *Atherosclerosis*, 271, 128–135. https://doi.org/10.1016/j.atherosclerosis.2018.02.022

Zhang, Y., Meng, T., Zuo, L., Bei, Y., Zhang, Q., Su, Z., … Yang, H. (2017). Xyloketal B attenuates fatty acid-induced lipid accumulation via the SREBP-1c pathway in NAFLD models. *Marine Drugs*, 15(6), 163. https://doi.org/10.3390/md15060163

Zhao, L., Varghese, Z., Moorhead, J. F., Chen, Y., & Ruan, X. Z. (2018). CD36 and lipid metabolism in the evolution of atherosclerosis. *British Medical Bulletin*, 126(1), 101–112. https://doi.org/10.1093/bmb/ldy006

Zhou, B., Zhou, D. L., Wei, X. H., Zhong, R. Y., Xu, J., & Sun, L. (2017). Astragaloside IV attenuates free fatty acid-induced ER stress and lipid accumulation in hepatocytes via AMPK activation. *Acta Pharmacologica Sinica*, 38(7), 998–1008. https://doi.org/10.1038/aps.2016.175

Health, Nutrition, & Food